Towards a model for predicting the macrostructure of multipass GTAW weld of austenitic stainless steel

Quentin Marsac, Cécile Gueudré, Marie-Aude Ploix, R. Robidet, A.L. Vetele, Gilles Corneloup, L. Forest, François Baque

Towards a model for predicting the macrostructure of multipass GTAW welds of austenitic stainless steel

Q. MARSAC [1,2,a], C. GUEUDRE [2], M.A. PLOIX [2], R.ROBIDET[3], A.L.VETELE[3] G. CORNELOUP [2], L.FOREST[3], F. BAQUE [1]

[1] CEA Cadarache DEN/DTN/STCP/LISM, Saint Paul Lez Durance, France

[2] Aix Marseille Université, CNRS, Centrale Marseille, LMA, UMR 7031, 4 impasse Nikola Tesla, CS 40006, 13453 Marseille Cedex 13, France

[3] DEN-Service d'études mécaniques et thermiques (SEMT), CEA, Université Paris-Saclay, F-91191 Gif-sur-Yvette, France

[a]quentin.marsac@cea.fr

Abstract

Ultrasonic testing of austenitic stainless steel multipass welds is complex. Because the welded structure is both anisotropic and heterogeneous, the propagation of the ultrasonic beam is disturbed (attenuation, deviation, splitting), making diagnosis difficult.

This diagnosis can be improved by modelling the ultrasonic propagation in the inspected weld. For this purpose, a description of the macrostructure is required. This can be obtained by optical means which provide a macrograph, but this involves a destructive cutting of the weld, or a weld sample. In the latter case, the sample must have been made and stored, and it must be representative of the inspected weld.

As an alternative, it is possible to predict the macrostructure of the weld by using a numerical model more or less realistic. For example, Ogilvy's model is an analytical model which predicts the macrostructure by considering a symmetrical structure of the weld. But this assumption is often non-realistic. Since 2000, EDF and the LMA develop another model called MINA which is a phenomenological model and so realistic one. MINA model predicts the macrostructure of Shielded Metal Arc Welding (SMAW) multipass welds, taking account information from welding conditions. It is then coupled to an ultrasonic simulation code, to simulate the impact of welding on ultrasonic propagation and therefore control.

In our study the welds are made with Gas Tungsten Arc Welding (GTAW) process. In this paper we first show that existing models are not adapted to this welding process. Then, we present the adopted scientific approach and the first advances aiming at the development of a new model relevant for GTAW welds.

Keywords: stainless steel multipass weld, GTAW, macrostructure modelling, grain growth, ultrasound, NDT.

1. Introduction

The primary circuit in pressurized water reactors includes numerous components, such as the vessel, the steam generator, the primary pumps, the pressurizer, interconnected by a piping system conveying high pressure and high temperature water. This is also the case of Sodium Fast Reactor structures. Most of these components are made of austenitic stainless steel, as it exhibits excellent corrosion resistance and very good mechanical strength at high temperature. Non-destructive examination aim at detecting potential defects in the numerous multipass welds present in the primary circuit and at characterizing them (position and dimensions), so that their severity can be assessed.

Ultrasonic testing makes it possible to detect and characterize defects regardless their orientation, but the results may be problematic to interpret, especially for those complex thick welds. A realistic prediction of the macrostructure should provide valuable insight into ultrasonic propagation through those complex structures and thereby allow a better controllability.

The mechanical behaviour of an austenitic weld is both anisotropic (grain elongation parallel to the lines of heat dissipation and preferential crystallographic direction) and heterogeneous (variation of grain orientation in the welded volume), see example on Figure 1a. The non-destructive ultrasonic testing of such welds reveals phenomena of deviation and splitting of the ultrasonic beam (Figure 1b), as well as attenuation and structure noise [1],[2].
Thereby to inspect such a weld by ultrasonic testing, those effects on ultrasound beam have to be predicted, by performing a numerical modelling that involves the knowledge of the macrostructure of the weld and a code simulating the ultrasonic propagation.

Numerous simulation codes of ultrasonic propagation are available in the literature to address the problem of ultrasonic testing of polycrystalline metals with both anisotropic and heterogeneous structures. Many of them are based on ray-tracing methods [3–6]. ATHENA code used here and developed by EDF is a finite element code that solves the elastodynamic equations, in the transient regime, in a heterogeneous and anisotropic medium [7,8]. The weld is described in ATHENA code by a finite number of homogeneous orthotropic domains (meshes), each domain being defined by a local grain orientation.

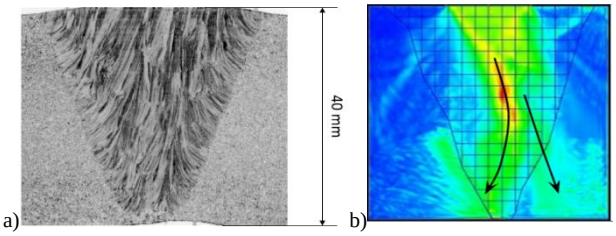

Figure 1 : a) Macrograph of a SMAW weld. b) Ultrasonic propagation simulated with ATHENA code: deviation and splitting of the ultrasonic beam.

The simulation requires a realistic description of the weld as input data: the geometry, the material and the macrostructure. Some models of grain structure at the macroscopic scale exist. Analytical ones consider a symmetrical description [3,9,10]. The phenomenological MINA model is more realistic but is relevant for SMAW (Shielded Metal Arc Welding) welds. These models are explained in the sections 2.1 and 2.2.

The welds studied here are made by a Gas Tungsten Arc Welding (GTAW) process, in flat position. In the section 2.3, Ogilvy and MINA models for GTAW welds are tested by comparing their results to macrographs, and highlighting their inadaptability. This is confirmed by the comparison of numerical and experimental ultrasonic propagation results.

Thereby we want to develop a new phenomenological model, relevant for GTAW process. The adopted scientific approach is then exposed and consists in beginning with analyses of specific GTAW mock-ups with well-chosen varying parameters. It will allow concluding on specific solidification mechanisms, and then provide the way to predict the macrostructure through a new phenomenological model.

2. Modelling of a weld structure

Several models have been developed to model the macrostructure of a weld, mainly following two approaches: the analytical one and the phenomenological one.

2.1. Analytical models

Ogilvy's model is the most commonly used for analytical model. The main and restrictive assumption of this model (like most of the analytical models) is the symmetry of the welded structure.

The local orientations of the grains are calculated as follow:

$$\theta_1(y,z) = \tan^{-1}\left(\frac{(T_1.(D_1+z.\tan(\alpha_1)))}{y^\eta}\right) \text{ (when y>0; } \theta_1 < 0).$$

$$\theta_2(y,z) = \tan^{-1}\left(\frac{(T_2.(D_2+z.\tan(\alpha_2)))}{y^\eta}\right) \text{ (when y<0; } \theta_2 > 0).$$

where α_1, α_2, D_1 and D_2 are defined by the geometry of chamfer, T_1, T_2 are the local grain orientations at the sloping edges and η is an evolution parameter of the local grain orientations from the sloping edges to the weld axis are refined in order to fit the real macrostructure (Figure 2).

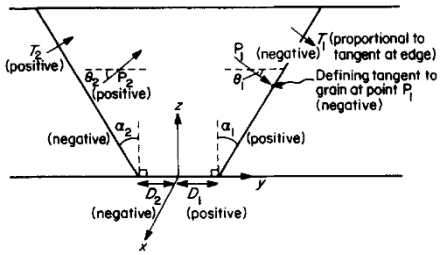

Figure 2 : Definition of parameters used in Ogilvy's model [3].

Those kinds of model were not sufficient to model welded structures as far as the result is obviously symmetrical, that is rarely the case in reality (see example of Figure 1a).

2.2. Phenomenological model MINA

The MINA model [11] was created for SMAW welds made in flat position. It allows a more realistic prediction of the grain orientations [12–15]. MINA model aims at predicting the grain growth direction in order to predict the real disturbances of the ultrasonic beam travelling through a weld.

It uses information from the welding notebook (describing the welding procedure and chamfer geometry). The main parameters of the welding procedure are as follows: number and sequencing order of passes, diameter of the electrodes, remelting rates and temperature gradient tilts.

It has been shown [16] that the first-order parameter which influences the most the welded structure is the sequencing order of passes. Figure 3 shows the four sequencing orders of passes.

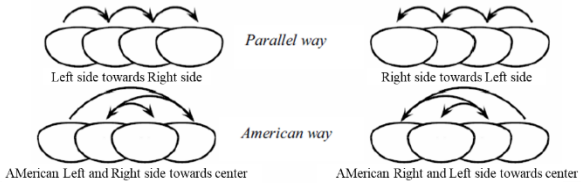

Figure 3 : Sequencing order of passes [16].

The MINA model exploits a proportionality rule between the electrode diameter and the pass thickness. Furthermore, MINA uses four parameters measured on macrographs: remelting parameters ($R_l = \frac{l}{L}$ « lateral » and $R_v = \frac{h}{H}$ « vertical ») and the temperature gradient tilt for a pass against the chamfer (θ_b) or against another pass (θ_c). The Figure 4 illustrates those four parameters.

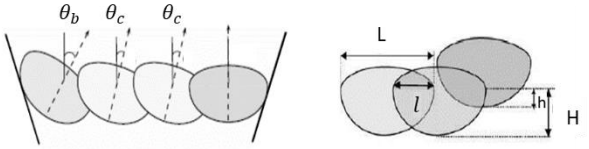

Figure 4 : Multipass welding with tilt parameters (left) and lateral and vertical remelting of a pass (right) [16].

The local grain orientation is predicted by an algorithm that takes into account the physical rules of epitaxial and selective growth together with the influence of the temperature gradient.
The austenite grains grow in an epitaxial mode: a grain grows from the neighbouring grain of the lower pass (with the same crystallographic direction) then tends to line up in the direction of the temperature gradient [17–20]. The phenomenon of selective growth implies that the columnar grains which crystallographic direction
< 1 0 0 > is close to the local direction of the temperature gradient grow faster than the neighbouring grains. The growth of the latter is therefore stopped [21,22].

2.3. Application on GTAW welds

In this section, the ability of those two models to predict the structure of a GTAW welds are tested. Figure 5 shows a macrograph of the GTAW weld considered here. The sequencing order of passes is American left and right side towards center for all layers.

Figure 5: Macrograph of GTAW weld

One can first observe that the macrostructure of this weld is relatively symmetrical. This is induced by the "American" sequencing order of passes.
The values of parameters of Ogilvy's model were chosen by optimisation in order to minimize the discrepancies with the macrographs. They are: $\alpha_1=\alpha_2=35°$, $D_1=D_2=1.5$ mm, $T_1=-T_2=-0.5$, $\eta=0.8$. The chosen values of parameters of MINA model were measured on a macrograph and are: $R_l=0.45$, $R_v=0.4$, $\theta_b=27.7°$, $\theta_c=23.7°$.

Figures 6 and 7 show at the top the prediction of the macrostructure by Ogilvy's model (Figure 6) and by MINA model (Figure 7), and at the bottom the comparison with the grain growth directions measured on the macrograph of figure 5 and predicted by models (Ogilvy's model (figure 6) and MINA model (figure 7)).

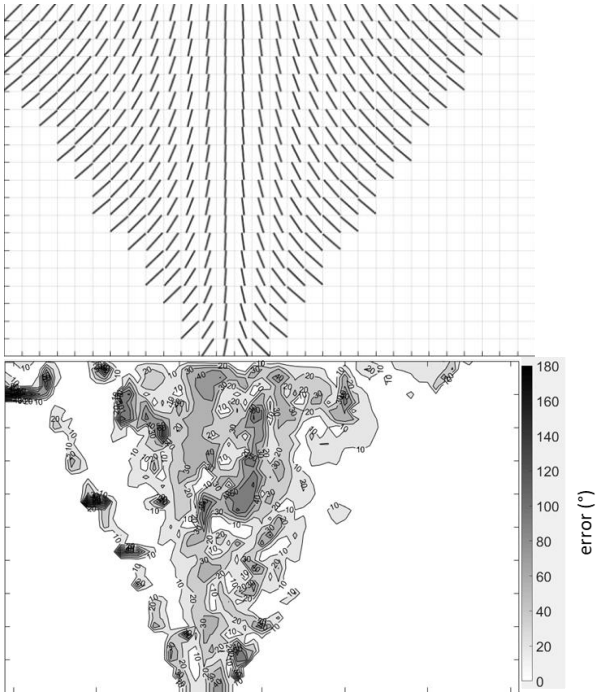

Figure 6: Prediction of grain growth directions by Ogilvy's model (top) and comparison between Ogilvy's model and macrograph (bottom).

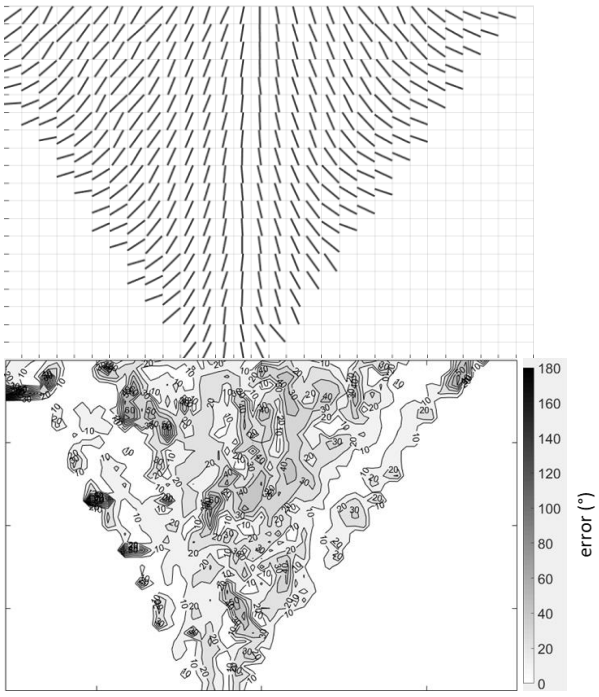

Figure 7: Prediction of grain growth directions by MINA model (top) and comparison between Ogilvy's model and macrograph (bottom).

The mean error between Ogilvy's model and macrograph is about 18° (with a standard deviation of 15.9°). The mean error between MINA model and macrograph is about at 19° (with a standard deviation of 14.8°).

We observe here that the results are very similar, with a quite high mean error. Usually, in the SMAW case, the mean error is rather about 10°-12°, with the standard deviation about 8°-10° [11,23].

In order to confirm the fact that these models are not adapted to GTAW welds, we now compare the ultrasonic results obtained experimentally on the one hand, and numerically on the other hand, by using MINA result as input data for ATHENA finite element code. As the mean error of the models are quite similar, we only consider MINA result.

This experience was performed in immersion with two transducers in transmission.

Figure 8 illustrates the principle of measurement. The two transducers (emitter and receiver) and the weld mock-up are immerged in water. During the measurement, the emitter is placed at a fixed position, in total, at five positions (-8, -4, 0, +4, +8 mm from the weld axis).
The receiver scans the opposite surface to measure the ultrasonic field transmitted over 70 mm (-35 mm to +35 from the weld axis) with a step of 0.5 mm.

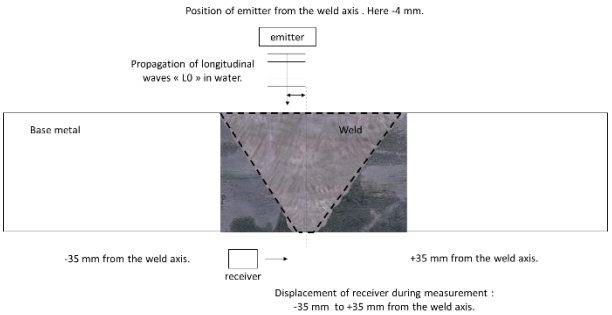

Figure 8: Principle of ultrasonic measurement in immersion, in transmission with two transducers.

At each location of the receiver, the maximum of acoustic amplitude is registered, and we obtain a so-called echodynamic.

The Figure 9 shows the two resulting echodynamics (red : experimental and blue : numerical (MINA model + ATHENA)) for position "-4" of the emitter.

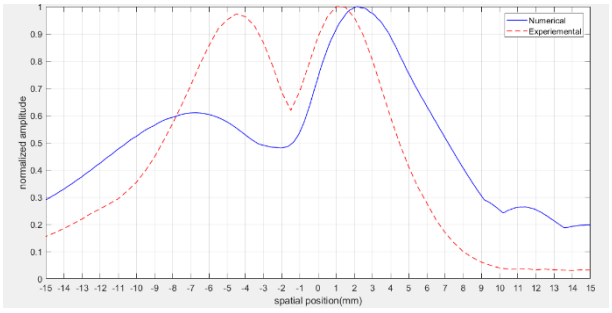

Figure 9 : Experimental and numerical echodynamics at position "-4" of the emitter.

As we observe, the difference between measured and predicted amplitudes is high. The simulation present several discrepancies with experience (in particular position and amplitude of the peaks). Thus, we show here the necessity of developing a new model for GTAW welds to improve the prediction.

3. Specificities of GTAW welds

As we have noted, Ogilvy's model or MINA model are not able to well predict the macrostructures of GTAW welds. In this part, we expose the specificities of GTAW welds.

We observe on GTAW welds macrographs that the grain growth direction is overall orthogonal to the boundary of the passes (Figure 10). Consequently, the shape of pass boundary has a high impact on grain growth direction as it was observed for SMAW welds [11].

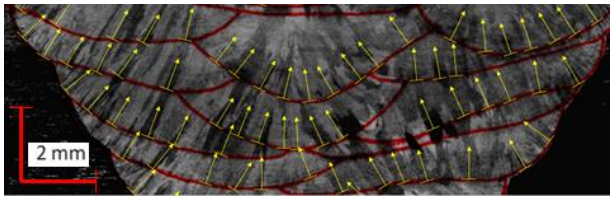

Figure 10 : GTAW weld macrograph (yellow arrows represents the grain growth direction at the boundaries of passes).

We present in this part, a summary of the state of art regarding the impact of welding parameters on the shape of pass boundary.

The heat transfer from the arc plasma to the weld pool and fluid flow in the weld pool determine the weld profile in the arc welding process [24,25].
Figure 11 illustrates the fluid flow in the weld pool and the arc plasma transfer. There are four driving forces of fluid flow in the weld pool: the Marangoni effects (surface tension), the Lorentz force (welding current), the buoyancy force (temperature gradient within the weld pool) and the drag force (velocity of shielding gas).

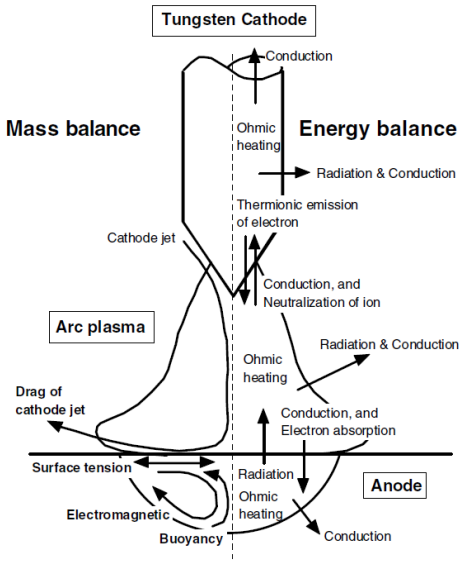

Figure 11 : Illustration of the four driving forces of fluid flow in the weld pool and arc plasma transfer [25].

As we noted, several welding parameters could modify the shape of pass boundary by the heat transfer from the arc plasma to the weld pool and fluid flow in the weld pool like welding voltage, intensity and speed, flow rate and type of shielding gas, and thus base metal and filler designation.

Figure 12 shows the effect of sulphur content in base metal on the shape of pass boundary.

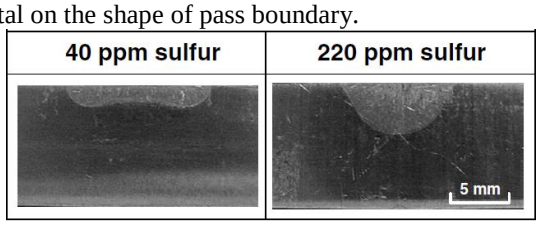

Figure 12 : The effect of sulphur rate in base metal on the shape of pass boundary [25].

It is clearly noted that shape of pass boundary is different: a low sulphur content generates a wide and shallow weld pool whereas a high sulphur content which generates a narrow and deep weld pool.
That is due to Marangoni effects, and as we noted, these effects are stimulated by surfactant elements as sulphur by surface tension gradient which depends on temperature.
In our case, the sulphur content in base metal and filler metal is around 20 ppm and surface tension gradient is relatively constant on a large bandwidth of temperature. Thus, the Marangoni effects are very low.
Mills and al [26], achieve to explain the variable weld penetration (shape of pass boundary) by three causes:

1. Alterations to the arc characteristics (welding voltage, intensity, type of shielding gas, …).
2. Changes in liquid/vapor or solid/vapor interfacial energy.
3. Differences in the direction of fluid flow in the weld pool, produced by surface tension gradients (sulphur content or other active elements).

Nestor [27] measured the distribution of heat intensity and current density at the anode of high current. By this way, he demonstrated the impact of several welding parameters (welding intensity, arc length, tip of electrode, …) on heat intensity and current density distributions and so on shape of pass boundary. Furthermore, he studied the effect of type of shielding gas on welding parameters like arc voltage, arc length, …

Evans and al [28] had showed that the relationships between welding voltage and arc length is linear (if welding voltage increase, the arc length increase).

Following this bibliographic work, an exhaustive list of the most influential welding parameters on the shape of pass boundary is proposed:

- Intensity, voltage and welding speed.
- Type of current, polarity.
- Diameter and tip of electrode, nozzle and filler metal diameter.
- Inclination of the torch and filler metal.
- Base metal, electrode and filler metal designation.
- Sequencing order of passes, welding position.
- Sweeping of the pass (amplitude and speed).
- Flow rate and type of shielding gas.
- Wire feed rate.
- Cold or hot wire.
- Rate deposition

To summary GTAW process has got globally three times more parameters than SMAW process.

In order to understand the effects of these welding parameters on the macrostructure (direction of grain growth), we manufactured several welds mock-ups. By analysing macrographs of these welds, it will be possible to conclude on the effect of these parameters.

4. Towards a new model for predicting macrostructure of GTAW welds : elaboration of new mock-ups

The scientific approach adopted to study the effects of the welding parameters is to manufacture several mock-ups by modifying some well-chosen parameters and analysing their macrographs. At a first step, we choose to study the effect of the most five important welding parameters on the macrostructure among the many ones listed above: welding intensity, voltage and welding speed, sweeping of the pass and wire feed rate. The Table 1 shows a review of varying parameters of the six GTAW mock-ups.

For all of these mock-ups the following parameters are identical: the type of current is direct and the polarity is Direct Current Electrode Negative (DCEN), together with the geometry of chamfer (V-shaped groove welds), base metal designation (316 L(N)), the filler metal designation and the sequencing order of passes (American Left Right).

Reference & description	Welding intensity	Welding voltage	Welding speed	Wire feed rate	Sweeping pass
1: Llow energy	Low	Low	Interme-diate	Interme-diate	No
2: Medium energy	High	High	Interme-diate	Interme-diate	No
3: Low energy	High	High	High	Interme-diate	No
4: High energy (higher than 2)	High	High	Low	Interme-diate	No
5: Low wire feed rate and no sweeping pass	High	High	Interme-diate	Low	No
6: Low wire feed rate and sweeping pass	High	High	Interme-diate	Low	Yes

Table 1 : Review of qualitative parameters of the six GTAW welds.

5. Conclusion

In this paper, we highlighted that both MINA model and Ogilvy's model are not able to predict properly the macrostructure of GTAW welds. The prediction of disturbance effects of the ultrasonic beam in order to inspect GTAW welds will be performed by developing a new phenomenological model.

Thanks to representative mock-ups, with well-chosen varying parameters, it will be possible to analyse the effects of welding parameters on the macrostructure and solidification mechanisms.

By this way, we will have a better understanding for developing a new phenomenological model.

The validation process of this model will be performed by comparing the orientations evaluated by the model with those measured on macrographs and then by comparing ultrasonic simulation results and experimental ones.

Acknowledgements

This project is funded by CEA.
GTAW welds are realized by the LTA (Laboratoire des Technologies d'Assemblages) of DEN-Service d'études mécaniques et thermiques (SEMT) at CEA Saclay.

References

[1] G. Corneloup, C. Gueudré, Non Destructive Testing and testability of materials and structures (Le contrôle non destructif et la contrôlabilité des matériaux et structures), Presses Polytechniques et Universitaires Romandes, 2017.

[2] B. Chassignole, R. El Guerjouma, M.A. PLOIX, T. Fouquet, Ultrasonic and structural characterization of anisotropic austenitic stainless steel welds: Towards a higher reliability in ultrasonic non-destructive testing, NDT E Int. 43 (2010) 273–282. doi:10.1016/j.ndteint.2009.12.005.

[3] J.A. Ogilvy, Computerized ultrasonic ray tracing in austenitic steel, NDT Int. 18 (1985) 67–77. doi:10.1016/0308-9126(85)90100-2.

[4] S.R. Kolkoori, M.U. Rahman, P.K. Chinta, M. Ktreutzbruck, M. Rethmeier, J. Prager, Ultrasonic field profile evaluation in acoustically inhomogeneous anisotropic materials using 2D ray tracing model: Numerical and experimental comparison, Ultrasonics. 53 (2013) 396–411. doi:10.1016/j.ultras.2012.07.006.

[5] O. Nowers, D.J. Duxbury, B.W. Drinkwater, Ultrasonic array imaging through an anisotropic austenitic steel weld using an efficient ray-tracing algorithm, NDT E Int. 79 (2016) 98–108. doi:10.1016/j.ndteint.2015.12.009.

[6] H. Zhou, Z. Han, D. Du, Y. Chen, A combined marching and minimizing ray-tracing algorithm developed for ultrasonic array imaging of austenitic welds, NDT E Int. 95 (2018) 45–56. doi:10.1016/j.ndteint.2018.01.008.

[7] E. Becache, P. Joly, C. Tsogka, Fictitious domains, mixed finite elements and perfectly matched layers for 2-d elastic wave propagation, J Comput Acoust. 9 (2001) 1175–1201. doi:10.1142/S0218396X01000966.

[8] E. Becache, P. Joly, C. Tsogka, An Analysis of New Mixed Finite Elements for the Approximation of Wave Propagation Problems, SIAM J. Numer. Anal. 37 (2000) 1053–1084. doi:10.1137/S0036142998345499.

[9] M. Spies, Modeling of transducer fields in inhomogeneous anisotropic materials using Gaussian beam superposition, NDT E Int. 33 (2000) 155–162. doi:10.1016/S0963-8695(99)00036-5.

[10] K.J. Langenberg, R. Hannemann, T. Kaczorowski, R. Marklein, B. Koehler, C. Schurig, F. Walte, Application of modeling techniques for ultrasonic austenitic weld inspection, NDT E Int. 33 (2000) 465–480. doi:10.1016/S0963-8695(00)00018-9.

[11] J. Moysan, A. Apfel, G. Corneloup, B. Chassignole, Modelling the grain orientation of austenitic stainless steel multipass welds to improve ultrasonic assessment of structural integrity, Int. J. Press. Vessels Pip. 80 (2003) 77–85. doi:10.1016/S0308-0161(03)00024-3.

[12] O. Nowers, D.J. Duxbury, B.W. Drinkwater, Ultrasonic array imaging through an anisotropic austenitic steel weld using an efficient ray-tracing algorithm, NDTE Int. 79 (2016) 98–108. doi:10.1016/j.ndteint.2015.12.009.

[13] Z. Fan, M.J.S. Lowe, Investigation of ultrasonic array measurements to refine weld maps of austenitic steel welds, AIP Conf. Proc. 1430 (2012) 873–880. doi:10.1063/1.4716316.

[14] Z. Fan, A.F. Mark, M.J.S. Lowe, P.J. Withers, Nonintrusive Estimation of Anisotropic Stiffness Maps of Heterogeneous Steel Welds for the Improvement of Ultrasonic Array Inspection, IEEE Trans. Ultrason. Ferroelectr. Freq. Control. 62 (2015) 1530–1543. doi:10.1109/TUFFC.2015.007018.

[15] J. Moysan, C. Gueudré, M.-A. Ploix, G. Corneloup, P. Guy, R.E. Guerjouma, B. Chassignole, Advances in ultrasonic testing of austenitic stainless steel welds. Towards a 3D description of the material including attenuation and optimisation by inversion, in: A. Leger, M. Deschamps (Eds.), Ultrason. Wave Propag. Non Homog. Media, Springer Berlin Heidelberg, 2009: pp. 15–24.

[16] C. Gueudré, L. Le Marrec, M. Chekroun, J. Moysan, B. Chassignole, G. Corneloup, Determination of the order of passes of an austenitic weld by optimization of an inversion process of ultrasound data, AIP Conf. Proc. 1335 (2011) 639–646. doi:10.1063/1.3591910.

[17] C.A. Gandin, M. Rappaz, A coupled finite element-cellular automaton model for the prediction of dendritic grain structures in solidification processes, Acta Metall. Mater. 42 (1994) 2233–2246. doi:10.1016/0956-7151(94)90302-6.

[18] O. Grong, Metallurgical Modelling of Welding, 2nd edition, The Institute of Materials, London, 1997.

[19] J.A. Brooks, K.W. Mahin, CHAPTER 2 - Solidification and Structure of Welds, in: D.L. Olson, R. Dixon, A.L. Liby (Eds.), Mater. Process. Theory Pract., Elsevier, 1990: pp. 35–78. doi:10.1016/B978-0-444-87427-6.50008-3.

[20] D.N. Lee, K. Kim, Y. Lee, C.-H. Choi, Factors determining crystal orientation of dendritic growth during solidification, Mater. Chem. Phys. 47 (1997) 154–158. doi:10.1016/S0254-0584(97)80044-2.

[21] W.F. Savage, C.D. Lundin, T. Chase, Solidification of fusion welds in face-centered cubic metals, Weld J. 47 (1968) 522s.

[22] H. Nakagawa, M. Katoh, F. Matsuda, T. Senda, Crystallographic Investigation for Origination of New Columnar Crystal in Aluminum Weld Metal Using Single Crystal Sheet :, Trans. Jpn. Weld. Soc. 2 (1971) 1–9.

[23] A. Apfel, J. Moysan, G. Corneloup, M. Fouquet, B. Chassignole, Coupling an ultrasonic propagation code with a model of the heterogeneity of multipass welds to simulate ultrasonic testing, Ultrasonics. 43 (2005) 447–56. doi:10.1016/j.ultras.2004.09.004.

[24] M. Tanaka, T. Shimizu, T. Terasaki, M. Ushio, F. Koshi-ishi, Y. C.-L, Effects of activating flux on arc phenomena in gas tungsten arc welding, Sci. Technol. Weld. Join. 5 (2000) 397–402. doi:10.1179/136217100101538461.

[25] M. Tanaka, J.J. Lowke, Predictions of weld pool profiles using plasma physics, J. Phys. Appl. Phys. (2007).

[26] K.C. Mills, B.J. Keene, Factors affecting variable weld penetration, Int. Mater. Rev. 35 (1990) 185–216. doi:10.1179/095066090790323966.

[27] O.H. Nestor, Heat Intensity and Current Density Distributions at the Anode of High Current, Inert Gas Arcs, J. Appl. Phys. 33 (1962) 1638–1648. doi:10.1063/1.1728803.

[28] D.M. Evans, D. Huang, J.C. McClure, A.C. Nunes, Arc effeciency of plasma arc welding, Weld. J. (1998) 53S–58S.